Local Air-Sea Interactions at Ocean Mesoscale and Submesoscale in a Western Boundary Current

Ehud Strobach, Patrice Klein, Andrea Molod, Abdullah A. Fahad, Atanas Trayanov, Dimitris Menemenlis, Hector Torres

Geophysical Research Letters

RESEARCH LETTER
10.1029/2021GL097003

Local Air-Sea Interactions at Ocean Mesoscale and Submesoscale in a Western Boundary Current

Ehud Strobach[1], Patrice Klein[2,3], Andrea Molod[4], Abdullah A. Fahad[4,5], Atanas Trayanov[4,6], Dimitris Menemenlis[7], and Hector Torres[7]

[1]Agricultural Research Organization, Rishon LeZion, Israel, [2]G.P.S. Division, California Institute of Technology, Pasadena, CA, USA, [3]LMD/IPSL, CNRS, Ecole Normale Supérieure, PSL Research University, Paris, France, [4]NASA, Goddard Space Flight Center, Greenbelt, MD, USA, [5]ESSIC, University of Maryland, College Park, MD, USA, [6]Science Systems and Applications Inc., Lanham, MD, USA, [7]Jet Propulsion Laboratory, California Institute of Technology, Pasadena, CA, USA

Abstract We present results from a new, global, high-resolution (~3-km for ocean and ~6-km for atmosphere) realistic earth system simulation. This simulation allows us to examine aspects of small-scale air-sea interaction beyond what previous studies have reported. Our study focuses on recurring intermittent wind events in the Gulf Stream region. These events induce local air-sea heat fluxes above Sea Surface Temperature (SST) anomalies with horizontal scales smaller than 500-km. In particular, strong latent heat bursts above warm SST anomalies are observed during these wind events. We show that such wind events are associated with a secondary circulation that acts to fuel the latent heat bursts by transferring dry air and momentum down to the surface. The intensity of this secondary circulation is related to the strength of small-scale SST fronts that border SST anomalies. The study of such phenomena requires high-resolution in both the atmospheric and oceanic components of the model.

Plain Language Summary We explore the atmospheric circulation above Sea Surface Temperature (SST) anomalies of less than 500 km-scale using a new, global, coupled ocean-atmosphere simulation performed at high horizontal resolution and integrated for 3 months. Our study focuses on intermittent wind events in the Gulf Stream region and the resulting local air-sea heat fluxes above warm SST anomalies: A strong latent heat burst above these SST anomalies is observed during the intermittent wind events. Furthermore, during these events, a secondary circulation develops up to altitudes of 2,000 m above warm SST anomalies, which results in sinking of warm and dry air and air momentum from upper levels down to the sea-surface. Such secondary circulation is triggered by the strong wind stress divergences that develop above small-scale SST fronts bordering the SST anomalies. The consequence is an increase of latent heat fluxes above SST anomalies.

Key Points:

- Strong turbulent flux discontinuities observed at ocean fronts suggest the importance of small scales for air-sea interactions
- Intermittent large-scale winds together with mesoscale Sea Surface Temperature variations trigger secondary circulations in the atmospheric boundary layer
- Air-sea interactions are explored under a wider range of periods and wind speeds than previously examined

Supporting Information:

Supporting Information may be found in the online version of this article.

Correspondence to:

E. Strobach,
udist@volcani.agri.gov.il

Citation:

Strobach, E., Klein, P., Molod, A., Fahad, A. A., Trayanov, A., Menemenlis, D., & Torres, H. (2022). Local air-sea interactions at ocean mesoscale and submesoscale in a Western Boundary Current. *Geophysical Research Letters*, *49*, e2021GL097003. https://doi.org/10.1029/2021GL097003

Received 16 NOV 2021
Accepted 11 MAR 2022

Author Contributions:

Conceptualization: Ehud Strobach, Patrice Klein
Data curation: Ehud Strobach
Formal analysis: Ehud Strobach
Funding acquisition: Andrea Molod, Dimitris Menemenlis
Investigation: Ehud Strobach, Patrice Klein, Andrea Molod, Abdullah A. Fahad
Methodology: Ehud Strobach
Project Administration: Ehud Strobach, Andrea Molod, Dimitris Menemenlis
Resources: Hector Torres
Software: Ehud Strobach, Atanas Trayanov, Hector Torres

1. Introduction

The physical climate system is fundamentally linked to the mechanisms that transport heat between the ocean interior and the upper troposphere across the air-sea interface. One major gateway for this transport is associated with the action of mesoscale Sea Surface Temperature (SST) anomalies with typical spatial scales of 50–500 km (Griffies et al., 2015; Siegelman et al., 2020; Su et al., 2018). These SST anomalies, reaching magnitudes of 2.5–3°C and bordered by sharp SST fronts at submesoscale (<50 km), are driven by the baroclinic instability in the ocean interior that produces mesoscale eddies, in particular in Western Boundary Currents (WBCs) and in the Antarctic Circumpolar Current (ACC) (Klein et al., 2019). In these regions, mesoscale eddies and submesoscale structures are thought to explain most of the upward vertical heat transport in the global ocean, up to 7*PW* close to the surface, leading to a cooling of the ocean interior and a warming of surface layers (Siegelman et al., 2020; Su et al., 2020). Such transport is balanced by the downward heat transport explained by the large-scale wind-driven circulation and small-scale diffusive processes (Griffies et al., 2015; Rackow et al., 2019).

Air masses passing over mesoscale SST anomalies are forced out of equilibrium as they encounter large differences between SST and air temperature. This is true only for SST anomalies with scales smaller than 500 km (Small et al., 2019), since at these scales air masses do not have enough time to adjust to SST changes. The resulting latent heat flux (LHF) anomalies, strongly intensified over warm SST anomalies, can exceed monthly magnitudes of 60 Wm^{-2} (Small et al., 2019), meaning that the ocean at mesoscale heats the atmosphere. WBCs

Supervision: Patrice Klein, Andrea Molod, Dimitris Menemenlis
Validation: Ehud Strobach, Atanas Trayanov
Visualization: Ehud Strobach, Abdullah A. Fahad
Writing – original draft: Ehud Strobach, Patrice Klein
Writing – review & editing: Ehud Strobach, Patrice Klein, Andrea Molod, Abdullah A. Fahad, Dimitris Menemenlis

and the ACC are colocated with the atmospheric storm tracks, which suggests a possible impact on the global atmospheric circulation through the intensified air-sea heat fluxes at the ocean mesoscale as suggested by Minobe et al. (2008) and O'Neill et al. (2017). Foussard, Lapeyre, and Riwal (2019), using an atmosphere-only model, showed that the latent heat release driven by mesoscale SST anomalies leads to a poleward shift of atmospheric storm tracks by up to 1,000 km. Ma et al. (2015) and Liu et al. (2021) pointed out that, through these processes, mesoscale eddies in the Kuroshio Extension have a remote influence on the rainfall over the West Coast of the U.S.. These studies did not include the impact of sharp SST fronts at submesoscales.

Idealized modeling studies with sub-kilometer resolution but no humidity (Sullivan et al., 2020; Wenegrat & Arthur, 2018) emphasize that intermittent wind blowing over warm mesoscale SST anomalies can lead to more intensified air-sea exchange when these anomalies are bordered by sharp SST fronts at submesoscale. An observational study (Shao et al., 2019) documented the strong discontinuity of the wind stress and surface heat fluxes across a sharp SST front 10 km-wide. These recent studies have however limited scope in terms of realism, temporal resolution, and range of wind speeds.

The present study revisits the impact of these sharp SST fronts on the air-sea exchange using a realistic global coupled ocean-atmosphere model, including humidity with kilometer-scale resolution and sub-hourly outputs. This model allows us to explore the impacts of mesoscale and submesoscale SST anomalies on the surface heat fluxes within a wider range of periods and wind speeds.

2. Model Description and Experimental Setup

The coupled model used in this study is the Goddard Earth Observing System infrastructure and atmospheric model coupled to the the Massachusetts Institute of Technology general circulation ocean model. The atmospheric model was configured to run with nominal horizontal grid spacing of 6 km and 72 vertical levels, while the ocean was configured to run with nominal horizontal grid spacing of 3 km and 90 vertical levels. The model simulation was initialized on 21 March. The results shown in this study are based on the 75 days segment of the simulation from 22 April to 6 June. More information on the main features of the coupled model (hereafter called GEOS-MITgcm) and the experimental setup can be found in Supporting Information S1.

3. Results

Our study focuses on the Gulf Stream (GS) region that hosts energetic mesoscale eddies. An example of the impact of mesoscale SST anomalies on the local atmospheric weather is shown in Figures 1a and 1b which emphasize the strong correspondence between the total turbulent heat fluxes at the sea surface (panel a) and the SST anomalies (panel b). Mesoscale SST anomalies are bordered by submesoscale SST fronts, with a ∼10 km width and an amplitude of up to ∼0.5°C per km (Figure 1b). Patterns of large turbulent heat fluxes, with magnitudes up to 500 W.m^{-2} (Figure 1a) display a strong discontinuity just above SST fronts, which is consistent with observation-based studies (e.g., Gula et al. (2014)). To understand how submesoscale SST fronts impact the interactions between the ocean and the atmosphere, we first analyze the relationship between these fronts and the wind stress curl and divergence. Next we describe the secondary circulation within the atmosphere in response to mesoscale and submesocale SST structures. Finally, we analyze the time and spatial scales involved in the resulting air-sea heat exchanges.

3.1. Wind Stress Curl and Divergence in Response to Submesoscale SST Fronts

Following previous studies (Chelton et al., 2004; Gaube et al., 2019; O'Neill et al., 2003), we first analyze the local atmospheric wind response to submesoscale SST fronts (∼10 km) in terms of the wind stress curl/divergence snapshots (see Section S2 in the Supporting Information S1). The snapshots on Figures 1c and 1d reveal that, with a strong background wind blowing from the northwest, the anomalies of local wind stress curl and divergence have a width close to that of SST fronts, and reach magnitudes up to ∼50 N.m^{-2} per 10,000 km (∼0.5 N.m^{-2} per Deg^{-1}). Unlike atmospheric convergence events, the wind stress curl and divergence patterns are relatively stationary in space (above the SST fronts) which indicate their connection to the front. Such magnitudes of wind

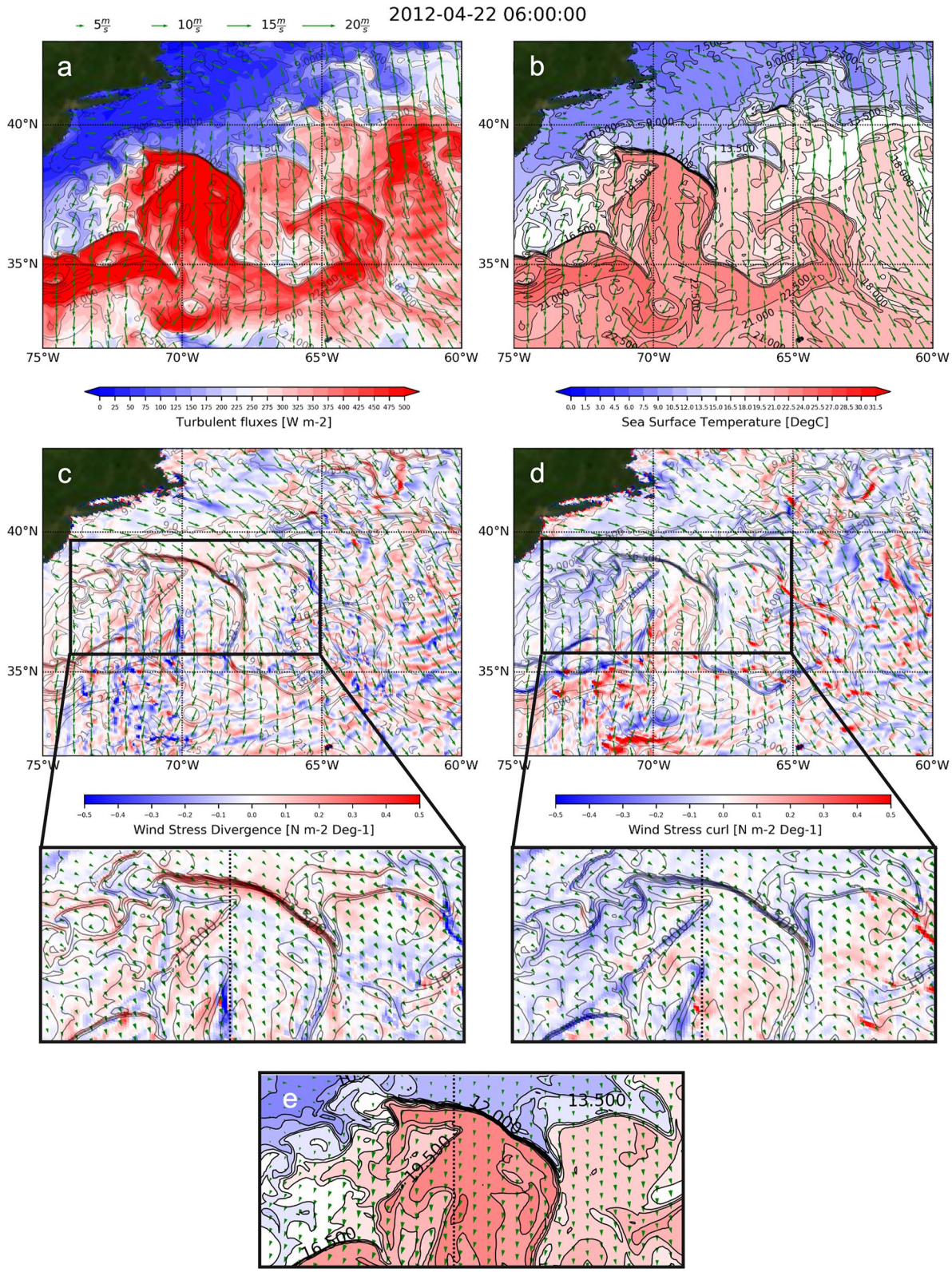

Figure 1. An overview over the Gulf Stream (GS) domain. (a and b) A snapshot of surface winds vectors overlaid on Turbulent fluxes (a) and Sea Surface Temperature (SST) (b) in the GS region. (c, d, and e) 24 hr mean (6–6 a.m.) surface winds (arrows) overlaid on wind stress divergence (c) and curl (d), and expended view over the SST front region (e).

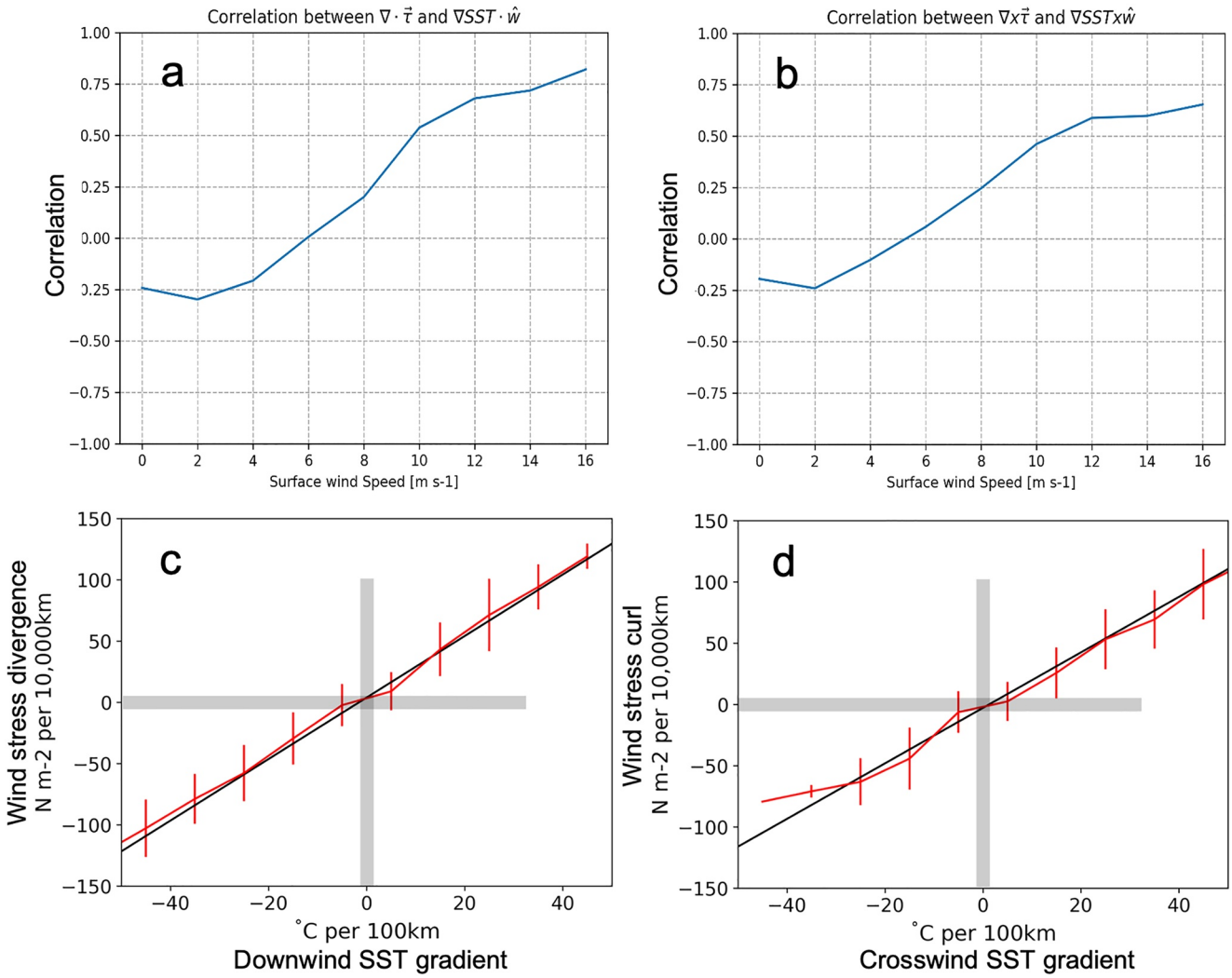

Figure 2. Correlation between the wind stress divergence and downwind Sea Surface Temperature (SST) gradient (a), and between the wind stress curl and crosswind SST gradient (b) as a function of the background surface winds. $\hat{w}$ is a unit vector pointing in the direction of the wind. (c and d): Binned scatter plots at high background wind conditions with error bars representing one standard deviation of the bin's scatter. Thick lines on panels c and d correspond to the range examined by Chelton et al. (2004).

stress curl/divergence snapshots are two orders larger than what is traditionally seen in monthly-mean lower-resolution observations (Chelton et al., 2004), and 10 times larger than snapshot results from coupled simulations with a resolution of only 25 km in the atmosphere (Foussard, Lapeyre, & Plougonven, 2019; Takatama & Schneider, 2017). The background wind speed and direction vary at time scales of one to several hours. A movie (not shown) reveals that the resulting local wind stress curl/divergence adjusts almost instantaneously. This emphasizes how the strength of SST fronts and time intermittent large-scale wind conditions impact the local wind response at submesoscale.

Figures 2a and 2b show the correlation between the windstress curl/divergence and the SST gradients (crosswind and downwind) as a function of the background surface wind speed. Correlations are positive and high with strong winds as expected from previous studies (Chelton et al., 2001, 2004; Foussard, Lapeyre, & Plougonven, 2019; O'Neill et al., 2003) but quickly decrease and become negative for wind speeds lower than 5 $m.s^{-1}$. The correlation patterns are consistent with Foussard, Lapeyre, and Plougonven (2019) who found that, with strong background winds, the wind stress curl/divergence correlate well with SST gradients, whereas with weak background winds they correlate with the Laplacian of the SST (as advocated by Lindzen and Nigam (1987) and Lambaerts et al. (2013)). In addition, the negative correlation is explained by the large magnitude of the

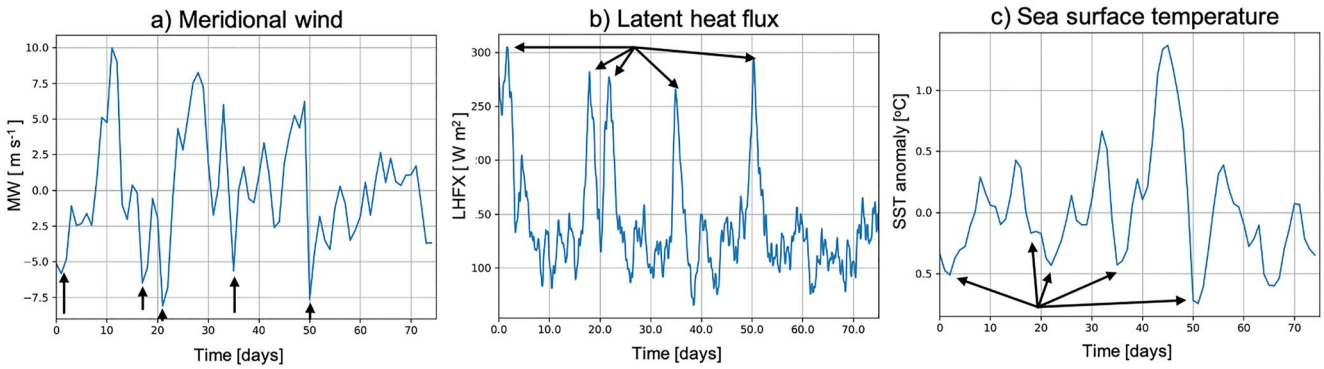

Figure 3. Time series of domain average meridional wind (a), latent heat flux (b), and Sea Surface Temperature (c). Black arrows represent the five latent heat burst events.

submesoscale SST fronts. Indeed, such strong SST fronts are known to be ageostrophic, leading to an opposite sign of the SST Laplacian and the SST gradient, as explained in Thomas et al. (2008).

Figures 2c and 2d further reveal the expected relationship between wind stress curl (and divergence) and SST gradients in the high wind speed regime (Chelton et al., 2004; Putrasahan et al., 2013; Takatama & Schneider, 2017). The slope is positive for both the wind stress curl and divergence indicating that the correlation with the SST gradient is mostly explained by moderate or strong winds. Values of these slopes are very close to those found in previous studies using coupled simulations with lower resolution (Foussard, Lapeyre, & Plougonven, 2019; Takatama & Schneider, 2017). However, the magnitudes of the windstress curl/divergence exceed ~1 $N.m^{-2}$ per Deg^{-1}, which is again more than 10–15 times larger than found in earlier studies. Such result emphasizes the significant impact of strong submesoscale SST fronts on the local wind response over 3 months. As shown by Chelton et al. (2004), the relationship between the windstress curl/divergence and SST gradients means that the local wind response over mesoscale eddies is intensified over warm eddies and decreased over cold eddies. The next section further explores the mechanisms involved in the local wind response at the mesoscale when such large values of the windstress curl/divergence are present.

3.2. Characteristics of the Local Atmospheric Response to SST Anomalies at Meso- and Submeso-Scales

Over the GS region, atmospheric weather includes numerous frontal synoptic systems characterized by cold air outbreaks off the east coast of the United States. These outbreaks typically last for 1–5 days and are associated with strong intermittent southward winds as illustrated in Figure 3a (see also Small et al. (2019)). Such intermittent wind events are intimately associated with strong LHF at the air-sea interface above warm SSTs that reach magnitudes of up to 300 $W.m^{-2}$ when averaged over the domain of (Figure 1). These fluxes lead to an SST decrease of up to 0.5°C (Figure 3c), which is much smaller than the magnitude of mesoscale SST anomalies.

We observed five strong wind events during our simulation period (see arrows on Figure 3), each one associated with a strong latent heat burst. Understanding the mechanisms that drive these LHF bursts requires a case by case study as the interactions are highly non-linear and front locations and strengths vary. In the rest of this section, we focus only on the first event, having in mind that the driving mechanisms are very similar for the other four. As illustrated in Figure 4, cold air at the surface crosses submesoscale SST fronts and quickly accelerates over warm SST anomalies, as seen by the increase in the arrow size south of 40°N near the SST maximum (Figure 4a). Above the atmospheric planetary boundary layer (APBL), the air-mass accelerates before the front (Figure 4b), as can be seen by the increase in arrow size north of 40°N. In these weather conditions, the APBL height over warm SST anomalies smoothly increases from ~200 m up to ~2,000 m, as depicted in Figures 4c and 4d (dotted lines). The lower APBL height north of the front reflects in part the sinking motion in the atmosphere associated with the secondary circulation (see the green arrows in Figures 4c and 4d). Also in Figures 4c and 4d, above the APBL at the transition region, the strong meridional wind increase before the front (blue blob in Figure 4) is associated with downward motion (positive omega). At the surface the opposite pattern is found—Wind slowdown before the front and speedup after the front. The horizontal wind anomalies are associated with downward motions as

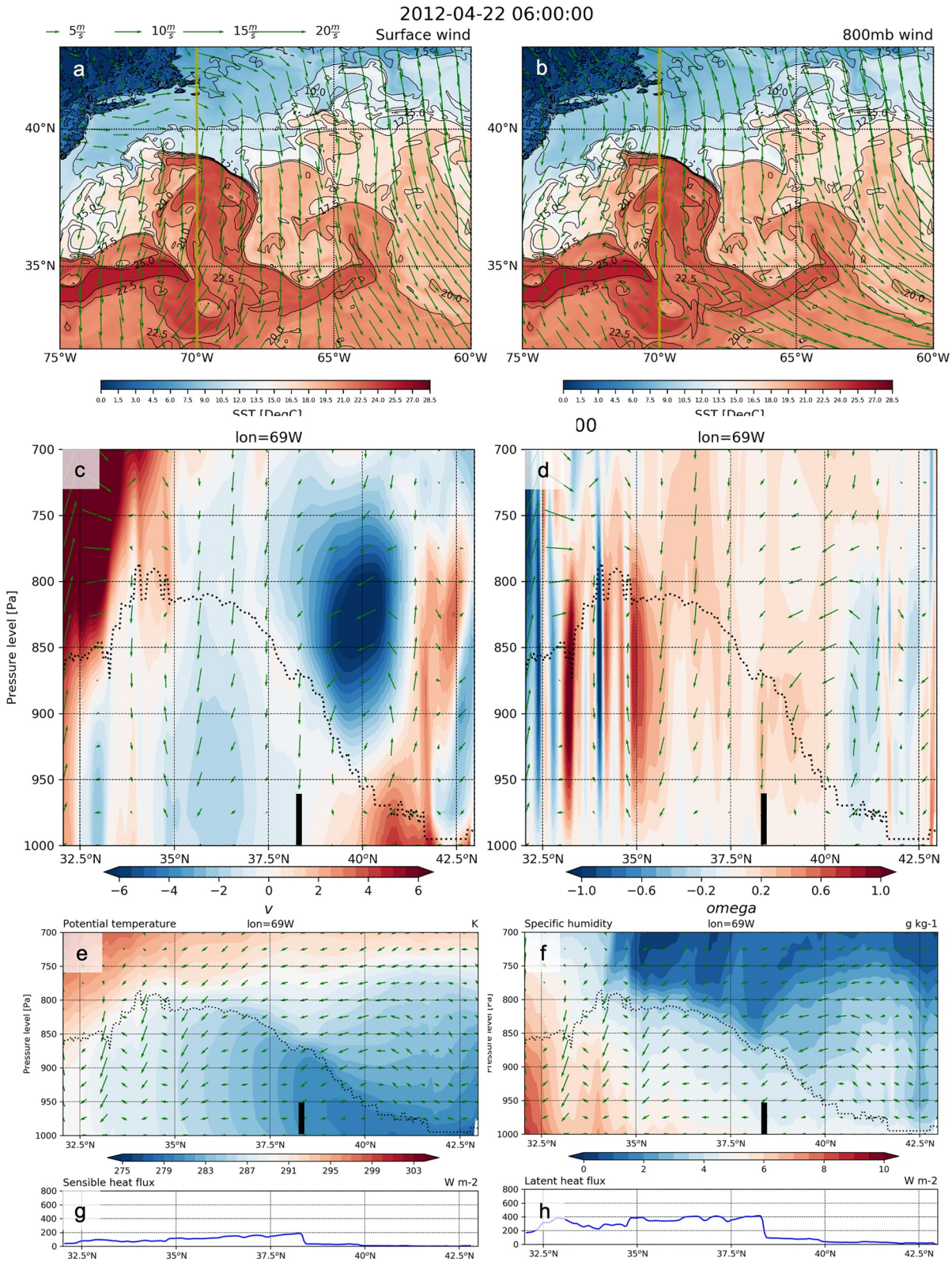

Figure 4. (a and b) A snapshot of surface (a) and 800mb (b) winds for the first latent heat burst event overlaid on Sea Surface Temperature (SST). (c and d) Vertical cross sections (lon = 69) of meridional wind anomaly with respect to the mean horizontal flow (c) and omega (d). Dashed black line depict the pressure level of the atmospheric planetary boundary layer. Black vertical lines denote the location of the SST front. Green arrows represent the wind vector normalized to the panel aspect ratio. (e and f) Potential temperature in shading, pressure level at the top of the planetary boundary layer in dotted black lines, and wind arrows. (g and h) Turbulent sensible and latent heat fluxes.

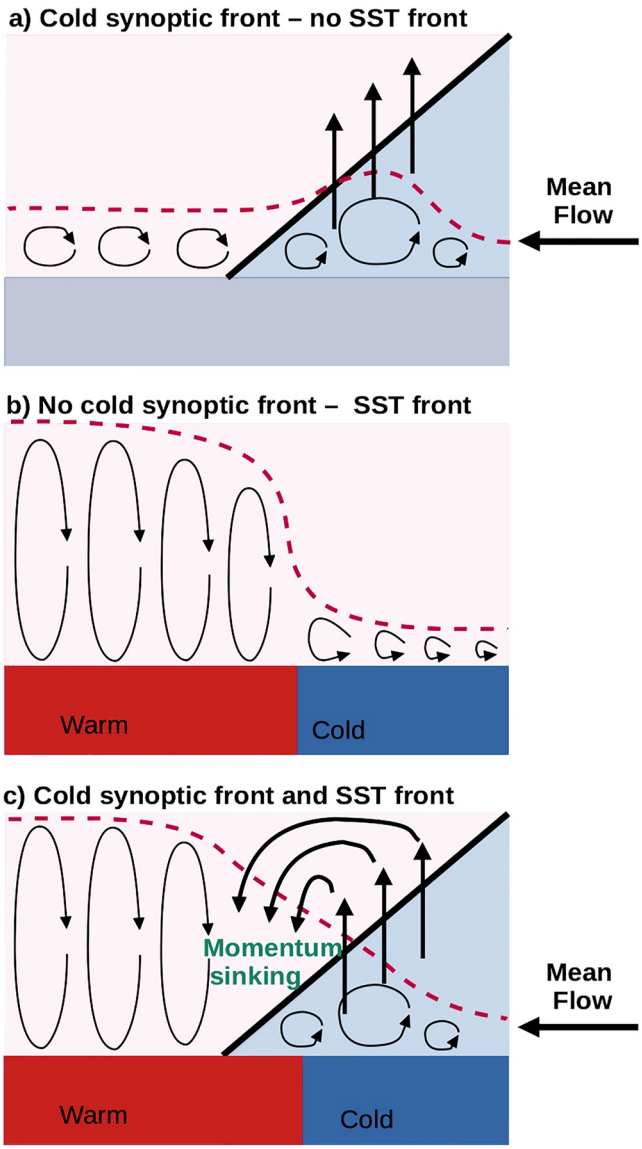

Figure 5. (a) Cold air-mass approaches an Sea Surface Temperature (SST) front (from right to left), the warmer air at the surface is pushed upward. No secondary circulation (b) Higher atmospheric planetary boundary layer forms above warmer SST due to higher mixing at no front conditions. No secondary circulation (c) Cold air-mass approaches to the front and produces momentum sinking above the front due to mixing. In all panels, the red dotted line represents the APBL height.

confirmed by Figures 4c and 4d. This is a consequence of the strong wind stress divergence triggered by the SST front, whose impact reaches an altitude of up to 2,500 m. Thus, in addition to the main surface wind that brings dry and cold air from the cold side of the front to the warm side, the secondary circulation results in sinking of warm and dry air from the upper levels down to the surface over warm SST (Figures 4e and 4f). This maintains the strong LHF and sensible heat flux (SHF) discontinuities just after the SST front as emphasized by Figures 4g and 4h and as also reported by Shao et al. (2019). Note that, from Figure 3b, the time scales associated with such events is to the order of some hours.

Figure 5 illustrates these mechanisms schematically. In the absence of an SST front, a cold air mass moving from the right will "dig" underneath warm air and push it upward (Figure 5a). In the SST front region, without the entrance of a cold air mass, a discontinuity in the APBL will be maintained. Higher APBL will form above warmer SST due to higher mixing (Figure 5b). When a cold air-mass approaches an SST front (Figure 5c), the warmer air at the surface will be pushed upward but, combined with mixing, will sink back bringing warmer but dryer air to the surface. The secondary circulation is found when SST front and synoptic system are acting together (panel c). This secondary circulation is similar to that described in previous studies (Kilpatrick et al., 2014; Sullivan et al., 2020; Wenegrat & Arthur, 2018). However the discrepancy between LHF and SHF mentioned above points to a specific impact of moist processes on the atmospheric response to submesoscale SST fronts. This impact has not been reported in these previous studies since they only considered a dry atmosphere.

3.3. Amplification of LHF Anomalies in a Fully Coupled System

Energetic wind and SST anomalies are usually characterized by different time and space scales; wind anomalies are dominated by spatial scales larger than 500 km and time scales smaller than 5 days, while SST anomalies are dominated by scales smaller than 500 km and time scales larger than 5 days (see spectra in the Supporting Information S1). The air-sea coupling causes SST anomalies to have an imprint on wind anomalies and vice-versa. As emphasized in the preceding section, mesoscale SST anomalies drive a local wind response at the same scales (due to the secondary circulation), with local wind speed increased (decreased) over warm (cold) SST anomalies. Similarly, large-scale time-intermittent wind stress anomalies are known to impact SST at the same scale (strong winds mix the upper ocean layer leading to negative large-scale SST anomalies). In this section we examine the consequences of these coupling mechanisms on LHF anomalies. For that purpose, LHF (Q_E) is expressed in terms of mechanical and thermal components

$$Q_E = \rho \cdot L_V \cdot CQ \cdot \Delta q \quad (1)$$

where ρ is the density of air and L_V the latent heat of vapourization. $CQ = u^* \cdot C_u \cdot C_q$ is the turbulent exchange coefficient for moisture, that contains a thermal component, C_q, the exchange coefficient for latent heat, and a mechanical component, $u^* \cdot C_u$, where u^* is the friction velocity and C_u is the exchange coefficient for momentum. $\Delta q = q_S - q_a$ also contains a thermal component, where q_a the air specific humidity and q_S the saturation specific humidity corresponding to SST. Positive Q_E means the ocean heats the atmosphere and vice-versa. The sign of Q_E is set by the sign of Δq.

Figure 6 shows the co-spectrum of CQ and Δq multiplied by L_V. The lower right part of the co-spectrum (red region) indicates a positive correlation between CQ and Δq. This is consistent with an increase of surface wind speed above warm SST anomalies, and with the secondary circulation (Figure 5) bringing dry air from aloft

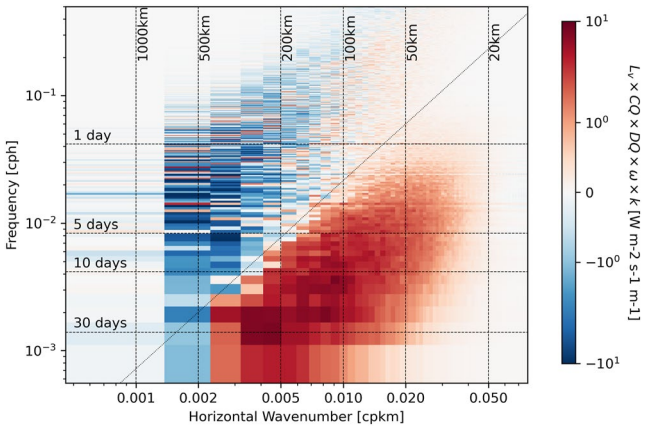

Figure 6. Co-spectrum of the latent heat fluxes. The co-spectrum is presented in a variance preserving form, which allows to directly compare the relative contribution of different time and space scales to the total covariance. See the Supporting Information S1 for the methodology to compute the co-spectrum. Note that DQ refers to Δq in the main text.

downward over the warm SST anomalies, all leading to larger positive Δq. Thus local imprints of warm SST anomalies on the atmosphere further heat the atmosphere because of the local wind speed increase and the secondary circulation. The same reasoning can be applied to cold SST anomalies, since both CQ and SST anomalies are negative.

In contrast, the upper left part of the co-spectrum (blue region) displays a negative covariance. Large-scale SST anomalies (>500 km) are weak (up to 0.5°C instead of up to 10°C for mesoscale anomalies), so the SST remains close to the air temperature. Upper ocean mixing by intermittent large-scale winds leads to cooler SST that becomes cooler than the air temperature and also to negative Δq anomalies. Figure 6 further points to the importance of the physics involved in the APBL and the ocean mixed-layer since that physics determines the imprints of one fluid on the other.

4. Conclusions

This study has investigated the high-frequency air-sea interactions at mid-latitudes, and more precisely, how the ocean locally impacts the atmosphere and vice-versa. On the one hand, large-scale SST anomalies (>500 km) have small magnitudes (up to 0.5°C at most) and, because of the large spatial scales, the atmosphere has time to adjust to the ocean SST (Small et al., 2019). This causes the atmosphere to drive the ocean such that a positive (negative) atmospheric wind anomaly leads to an increase (decrease) in vertical heat flux and a cooler (warmer) SST. The SST decrease or increase in response to the atmosphere (blue region on Figure 6) does not exist in an atmosphere only model (Gentemann et al., 2020; Small et al., 2019). On the other hand, mesoscale SST anomalies (<500 km) have large magnitudes (up to 10°C). Because of these smaller spatial scales, the temperature and humidity of air masses blowing over these anomalies have no time to adjust, leading to larger positive difference between warm SST anomalies and air temperature and therefore to larger upward surface heat fluxes (Gentemann et al., 2020; Minobe et al., 2008; O'Neill et al., 2017; Small et al., 2019). Our results further emphasize that when a southward strong wind is blowing across sharp SST fronts at submesoscale bordering these anomalies, it triggers a wind stress curl/divergence with large magnitude that forces a secondary circulation. This secondary circulation develops quickly, and leads to local wind intensification above warm mesoscale SST anomalies. Such local secondary circulations above warm SST anomalies further amplify LHF anomalies, and cause the ocean to further drive the atmosphere, as shown in the red region on Figure 6. Such feedback interactions between the ocean and atmosphere at these ocean mesoscales and submesoscales are not present in ocean-only models since both local wind and air humidity responses are lacking in these models.

This study extends the findings from recent 2-D idealized studies that use a dry atmosphere, and further stress the importance of resolving submesoscale features not only in the ocean but also in the atmosphere. The contribution of the resulting local LHF anomalies to the evolution of atmospheric weather still needs to be assessed over a longer time period and in the global ocean. The mechanisms reported in the present study are expected to be valid during other seasons, particularly during winter months when SST fronts are the strongest.

Acknowledgments
This research was made possible by grants from the NASA Modeling, Analysis, and Prediction and Physical Oceanography programs. Goddard Earth Observing System development was funded under NASA MAP-supported GMAO "core" funding. P. Klein, D. Menemenlis, and H. Torres carried out research at the Jet Propulsion Laboratory, California Institute of Technology, under contract with NASA. High-end computing resources were provided by the NASA Advanced Supercomputing (NAS) Division of the Ames Research Center. We are grateful for extensive support by the NAS Visualization & Data Analysis Group.

Data Availability Statement

Open research Data leading to this publication was made available as part of a Zenodo repository at: https://zenodo.org/record/5669247/#.YYyqy71BweU.

References

Chelton, D. B., Esbensen, S. K., Schlax, M. G., Thum, N., Freilich, M. H., Wentz, F. J., et al. (2001). Observations of coupling between surface wind stress and sea surface temperature in the eastern tropical Pacific. *Journal of Climate*, *14*(7), 1479–1498. https://doi.org/10.1175/1520-0442(2001)014<1479:oocbsw>2.0.co;2

Chelton, D. B., Schlax, M. G., Freilich, M. H., & Milliff, R. F. (2004). Satellite measurements reveal persistent small-scale features in ocean winds. *Science*, *303*(5660), 978–983. https://doi.org/10.1126/science.1091901

Foussard, A., Lapeyre, G., & Plougonven, R. (2019). Response of surface wind divergence to mesoscale SST anomalies under different wind conditions. *Journal of the Atmospheric Sciences*, *76*(7), 2065–2082. https://doi.org/10.1175/jas-d-18-0204.1

Foussard, A., Lapeyre, G., & Riwal, P. (2019). Storm tracks response to oceanic eddies in idealized atmospheric simulations. *Journal of Climate*, *32*, 445–463. https://doi.org/10.1175/jcli-d-18-0415.1

Gaube, P., Chickadel, C., Branch, R., & Jessup, A. (2019). Satellite observations of SST-induced wind speed perturbation at the oceanic submesoscale. *Geophysical Research Letters*, *46*(5), 2690–2695. https://doi.org/10.1029/2018gl080807

Gentemann, C. L., Clayson, C. A., Brown, S., Lee, T., Parfitt, R., Farrar, J. T., et al. (2020). Fluxsat: Measuring the ocean–atmosphere turbulent exchange of heat and moisture from space. *Remote Sensing*, *12*(11), 1796. https://doi.org/10.3390/rs12111796

Griffies, S. M., Winton, M., Anderson, W. G., Benson, R., Delworth, T. L., Dufour, C. O., et al. (2015). Impacts on ocean heat from transient mesoscale eddies in a hierarchy of climate models. *Journal of Climate*, *28*(3), 952–977. https://doi.org/10.1175/jcli-d-14-00353.1

Gula, J., Molemaker, M. J., & McWilliams, J. C. (2014). Submesoscale cold filaments in the gulf stream. *Journal of Physical Oceanography*, *44*(10), 2617–2643. https://doi.org/10.1175/JPO-D-14-0029.1

Kilpatrick, T., Schneider, N., & Qiu, B. (2014). Boundary layer convergence induced by strong winds across a midlatitude SST front. *Journal of Climate*, *27*(4), 1698–1718. https://doi.org/10.1175/JCLI-D-13-00101.1

Klein, P., Lapeyre, G., Siegelman, L., Qiu, B., Fu, L.-L., Torres, H., et al. (2019). Ocean-scale interactions from space. *Earth and Space Science*.

Lambaerts, J., Lapeyre, G., Plougonven, R., & Klein, P. (2013). Atmospheric response to sea surface temperature mesoscale structures. *Journal of Geophysical Research: Atmospheres*, *118*(17), 9611–9621. https://doi.org/10.1002/jgrd.50769

Lindzen, R. S., & Nigam, S. (1987). On the role of sea surface temperature gradients in forcing low-level winds and convergence in the tropics. *Journal of the Atmospheric Sciences*, *44*(17), 2418–2436. https://doi.org/10.1175/1520-0469(1987)044<2418:otross>2.0.co;2

Liu, X., Ma, X., Chang, P., Jia, Y., Fu, D., Xu, G., et al. (2021). Ocean fronts and eddies force atmospheric rivers and heavy precipitation in Western North America. *Nature Communications*, *12*(1), 1–10. https://doi.org/10.1038/s41467-021-21504-w

Ma, J., Xu, H., Dong, C., Lin, P., & Liu, Y. (2015). Atmospheric responses to oceanic eddies in the kuroshio extension region. *Journal of Geophysical Research: Atmospheres*, *120*(13), 6313–6330. https://doi.org/10.1002/2014jd022930

Minobe, S., Kuwano-Yoshida, A., Komori, N., Xie, S.-P., & Small, R. J. (2008). Influence of the gulf stream on the troposphere. *Nature*, *452*(7184), 206. https://doi.org/10.1038/nature06690

O'Neill, L. W., Chelton, D. B., & Esbensen, S. K. (2003). Observations of SST-induced perturbations of the wind stress field over the southern ocean on seasonal timescales. *Journal of Climate*, *16*(14), 2340–2354.

O'Neill, L. W., Haack, T., Chelton, D. B., & Skyllingstad, E. (2017). The gulf stream convergence zone in the time-mean winds. *Journal of the Atmospheric Sciences*, *74*(7), 2383–2412.

Putrasahan, D. A., Miller, A. J., & Seo, H. (2013). Isolating mesoscale coupled ocean–atmosphere interactions in the kuroshio extension region. *Dynamics of Atmospheres and Oceans*, *63*, 60–78. https://doi.org/10.1016/j.dynatmoce.2013.04.001

Rackow, T., Sein, D. V., Semmler, T., Danilov, S., Koldunov, N. V., Sidorenko, D., et al. (2019). Sensitivity of deep ocean biases to horizontal resolution in prototype cmip6 simulations with awi-cm1. 0. *Geoscientific Model Development*, *12*(7), 2635–2656. https://doi.org/10.5194/gmd-12-2635-2019

Shao, M., Ortiz-Suslow, D. G., Haus, B. K., Lund, B., Williams, N. J., Özgökmen, T. M., et al. (2019). The variability of winds and fluxes observed near submesoscale fronts. *Journal of Geophysical Research: Oceans*, *124*(11), 7756–7780. https://doi.org/10.1029/2019jc015236

Siegelman, L., Klein, P., Rivière, P., Torres, H. S., Thompson, A. F., Flexas, M., & Menemenlis, D. (2020). Enhanced upward heat transport at deep submesoscale ocean fronts. *Nature Geoscience*, *13*, 50–55. https://doi.org/10.1038/s41561-019-0489-1

Small, R. J., Bryan, F. O., Bishop, S. P., & Tomas, R. A. (2019). Air–sea turbulent heat fluxes in climate models and observational analyses: What drives their variability? *Journal of Climate*, *32*(8), 2397–2421. https://doi.org/10.1175/jcli-d-18-0576.1

Su, Z., Torres, H., Klein, P., Thompson, A. F., Siegelman, L., Wang, J., et al. (2020). High-frequency submesoscale motions enhance the upward vertical heat transport in the global ocean. *Journal of Geophysical Research: Oceans*, *125*(9), e2020JC016544. https://doi.org/10.1029/2020jc016544

Su, Z., Wang, J., Klein, P., Thompson, A. F., & Menemenlis, D. (2018). Ocean submesoscales as a key component of the global heat budget. *Nature Communications*, *9*(1), 775. https://doi.org/10.1038/s41467-018-02983-w

Sullivan, P. P., McWilliams, J. C., Weil, J. C., Patton, E. G., & Fernando, H. J. (2020). Marine boundary layers above heterogeneous SST: Across-front winds. *Journal of the Atmospheric Sciences*, *77*(12), 4251–4275. https://doi.org/10.1175/jas-d-20-0062.1

Takatama, K., & Schneider, N. (2017). The role of back pressure in the atmospheric response to surface stress induced by the Kuroshio. *Journal of the Atmospheric Sciences*, *74*(2), 597–615. https://doi.org/10.1175/jas-d-16-0149.1

Thomas, L. N., Tandon, A., & Mahadevan, A. (2008). Submesoscale processes and dynamics. *Ocean modeling in an Eddying Regime*, *177*, 17–38. https://doi.org/10.1029/177gm04

Wenegrat, J., & Arthur, R. (2018). Response of the atmospheric boundary layer to submesoscale sea surface temperature fronts. *Geophysical Research Letters*, *45*(24), 13–505. https://doi.org/10.1029/2018gl081034

References From the Supporting Information

Adcroft, A., & Campin, J.-M. (2004). Rescaled height coordinates for accurate representation of free-surface flows in ocean circulation models. *Ocean Modelling*, *7*(3–4), 269–284. https://doi.org/10.1016/j.ocemod.2003.09.003

Flexas, M. M., Thompson, A. F., Torres, H. S., Klein, P., Farrar, J. T., Zhang, H., & Menemenlis, D. (2019). Global estimates of the energy transfer from the wind to the ocean, with emphasis on near-inertial oscillations. *Journal of Geophysical Research: Oceans*. https://doi.org/10.1029/2018JC014453

Forget, G., Campin, J.-M., Heimbach, P., Hill, C. N., Ponte, R. M., & Wunsch, C. (2015). Ecco version 4: An integrated framework for non-linear inverse modeling and global ocean state estimation. *Geoscientific Model Development*, *8*(10), 3071–3104. https://doi.org/10.5194/gmd-8-3071-2015

Garfinkel, C. I., Molod, A. M., Oman, L. D., & Song, I.-S. (2011). Improvement of the geos-5 agcm upon updating the air-sea roughness parameterization. *Geophysical Research Letters*, *38*(18). L1870. https://doi.org/10.1029/2011GL048802

Gill, A. E. (1982). Atmosphere. *Ocean Dynamics*, *30*, 662.

Helfand, H. M., & Schubert, S. D. (1995). Climatology of the simulated great plains low-level jet and its contribution to the continental moisture budget of the United States. *Journal of Climate*, *8*(4), 784–806. https://doi.org/10.1175/1520-0442(1995)008<0784:COTSGP>2.0.CO;2

Large, W. G., McWilliams, J. C., & Doney, S. C. (1994). Oceanic vertical mixing: A review and a model with a nonlocal boundary layer parameterization. *Reviews of Geophysics*, *32*(4), 363–403. https://doi.org/10.1029/94RG01872

Marshall, J., Adcroft, A., Hill, C., Perelman, L., & Heisey, C. (1997). A finite-volume, incompressible Navier Stokes model for studies of the ocean on parallel computers. *Journal of Geophysical Research*, *102*(C3), 5753–5766. https://doi.org/10.1029/96JC02775

Molod, A., Suarez, M., & Partyka, G. (2013). The impact of limiting ocean roughness on geos-5 agcm tropical cyclone forecasts. *Geophysical Research Letters*, *40*(2), 411–416. https://doi.org/10.1029/2012GL053979

Qiu, B., Chen, S., Klein, P., Wang, J., Torres, H., Fu, L.-L., & Menemenlis, D. (2018). Seasonality in transition scale from balanced to unbalanced motions in the world ocean. *Journal of Physical Oceanography*, *48*(3), 591–605.

Savage, A. C., Arbic, B. K., Richman, J. G., Shriver, J. F., Alford, M. H., Buijsman, M. C., et al. (2017). Frequency content of sea surface height variability from internal gravity waves to mesoscale eddies. *Journal of Geophysical Research: Oceans*, *122*(3), 2519–2538. https://doi.org/10.1002/2016JC012331

Small, R. J., Bryan, F. O., Bishop, S. P., Larson, S., & Tomas, R. A. (2020). What drives upper-ocean temperature variability in coupled climate models and observations? *Journal of Climate*, *33*(2), 577–596.

Strobach, E., Molod, A., Trayanov, A., Forget, G., Campin, J.-M., Hill, C., & Menemenlis, D. (2020). Three-to-six-day air–sea oscillation in models and observations. *Geophysical Research Letters*, *47*(10), e2019GL085837. https://doi.org/10.1029/2019GL085837

Torres, H. S., Klein, P., Menemenlis, D., Qiu, B., Su, Z., Wang, J., et al. (2018). Partitioning ocean motions into balanced motions and internal gravity waves: A modeling study in anticipation of future space missions. *Journal of Geophysical Research: Oceans*, *123*(11), 8084–8105. https://doi.org/10.1029/2018JC014438